Resistive switching behavior in memristors with TiO_2 nanorod arrays of different dimensions

Yantao Yu[1,2], *Chunqi Wang*[1,2], *Chao Jiang*[*1,2], *Isaac Abrahams*[3], *Zuojuan Du*[1,2], *Qiancheng Zhang*[4], *Jia Sun*[4], *Xiaozhong Huang*[1,2].

[1] Institute of Aeronautics and Astronautics, Central South University, Changsha 410012, China

[2] Key Lab for Advanced Fibers and Composites of Hunan Province, Changsha 410012, China

[3] School of Biological and Chemical Sciences, Queen Mary University of London, London E1 4NS, UK

[4] Hunan Key Laboratory for Super Microstructure and Ultrafast Process, School of Physics and Electronics, Central South University, Changsha, Hunan 410083, China

*Corresponding author: **jiangchao@csu.edu.cn** (Chao Jiang)

ABSTRACT: In this work, memristors based on TiO_2 nanorod arrays (TNAs) were fabricated using a hydrothermal synthesis method. The memristors had a structure consisting of a TNA sandwiched between gold and fluorine doped tin oxide (FTO) coated glass. Devices were constructed using TNAs containing nanorods of different height, diameter and area ratio, with different oxygen vacancy concentrations. The devices exhibit resistance switching behavior and the current through the devices is related to the oxygen vacancy concentration and the area ratio of TNAs. When the height of nanorods is around 3 μm or less, the devices perform well with a current that is as low as 10^{-8} A in the high resistance state (HRS) and 10^{-4} A in the low resistance state (LRS). It is found that the space charge limited current (SCLC) mechanism associated with the oxygen vacancies explains the current-voltage behavior of these devices in this three layer structure. A schematic model is presented to illustrate the changes in oxygen vacancy concentration and switching processes, including the formation of new oxygen vacancies (triggered vacancies) to explain the large increase in current at the end of the setting process in these devices.

KEY WORDS: Memristors, TiO_2 nanorod arrays, Area ratio, SCLC mechanism.

Introduction

Titanium dioxide is used many applications in the fields of semiconductors [1], photo catalysts [2-4], dielectric capacitors[5], paints [6], and dye-sensitized solar cells [7-9]. Memristor devices based on TiO_2 show non-volatile and non-linear behavior and constitute a promising approach to breaking Moore's law and igniting a new research field [10-12]. The behavior of memristors with a metal/insulator/metal structure allows for the design of new electronic devices. The stability and current/voltage properties of such devices suggest a promising future for applications in large scale intelligent integrated systems, namely bio-synapse emulators products， resistive random access memory (RRAM) and also as an alternative for flash memory [13-15]. Novel and stable structures, suitable for memristor devices, have been extensively researched in the electrical engineering field. Several researchers have focused their work on metal oxide memristors including ZnO [16], TiO_2 [17], HfO_2 [18], NiO [19], and CuO [20]. The active layer structure of memristor devices in previous research based on TiO_2 can be mainly separated into cross point and intact thin films, which both show hysteretic current-voltage (I-V) behavior or analog switching [21-23]. There are also some investigations on resistive switching characteristics of TiO_2 nanowires [24] and TiO_2 nanorods [25], including neuromorphic behavior [26]. Unlike thin films fabricated by physical sputtering, for which post-annealing is needed to introduce oxygen vacancies, hydrothermally

fabricated TiO_2 nanorod arrays (TNAs) contain significant oxygen vacancy concentrations after low temperature fabrication [14]. The structure of TNAs produced in this way consists of individual nanorods separated from each other and is different to the structure of intact films. Generally, beam lithography techniques can then been used to construct word and bit lines required for memristor devices [27]. After depositing crossbar electrode arrays upon TNAs, another layer can be synthesized and lapped to fabricate multiple layer devices using a low temperature hydrothermal process.

A number of mechanisms have been proposed to account for the switching behavior in TiO_{2-x} memristors. Szot et al. [12] have classified these broadly into four catagories, viz: electrochemical where the switching is based on ionic diffusion and/or change in valency on the cation sublattice [28, 29]; thermochemical involving formation and rupture of conducting filaments as a result of local temperature changes [30]; pure electronic where the memristor behaves as a Schottky type diode [13] and finally the phase change mechanism involving the formation of more highly conducting Magnèli phases such as Ti_4O_7 [12]. Thus mechanisms may involve ionic and/or electronic transport and be unipolar or dipolar. Devices based on hydrothermally produced TiO_2 nanorods ave been shown to have excellent continuous switching properties [31]. The low temperature synthesis of the TNAs affords are high concentrations of oxygen vacancies, which can participate in the switching

mechanism. For these types of systems, with high vacancy concentrations, a trap-mediated space-charge-limited current (SCLC) model has been proposed [31]. Electron trapping occurs on the vacancies at the interface between the individual nanorods, which induces the formation of channels for electron mobility.

To date work on TNA-based systems has focused mainly on the resistive switching behavior and mechanism, but there has been little reported on the influence of nanorod dimensions on the intrinsic behavior of these systems. In this work, we seek to verify the hypothesis that nanorod dimensions can have a significant influence on memristive behaviour in TNA based devices. We show that nanorod arrays with different rod dimensions can be readily fabricated using a low cost hydrothermal method by adjusting the temperature. The hydrothermal process [32-36]is an easier and more controllable way to obtain well aligned arrays than other techniques, such as atomic layer deposition [37] and sputtering [38]. This method yields nanorod layers where the rods are aligned perpendicular to the substrate and the rod dimensions can be tuned by altering temperature and process duration. Electrical characterization of memristors constructed from these TNAs is presented and their switching behavior is discussed in detail, in terms of the space charge limited current (SCLC) hypothesis.

Experimental

The TiO_2 nanorod arrays were fabricated by a hydrothermal synthesis process under a pressurized air atmosphere. Four pieces of fluorine doped tin oxide (FTO) coated

glass (supplied by Kaivo Optoelectronic Technology Co., Ltd.) substrate were successively immersed in acetone, ethyl alcohol, deionized water and were ultrasonically cleaned thoroughly for 15 min. The clean FTO substrates (blown by nitrogen gas to remove any surface dust) were located in a 20 ml Teflon sealed autoclave container with the conductive surface of the FTO leant against the wall of container. The bath solution consisted of 5 ml H_2O, 5 ml concentrated HCl (37 w/w%) and 0.238 ml titanium butoxide, which was mixed and stirred for 30 min before placing in the reactors. The sealed container was placed in an oven and heated over a period of 25 min to the set temperature. The hydrothermal process employed four different temperatures (413 K, 433 K, 453 K or 473 K) and held for 2 h to allow the growth of the TNAs on the glass substrate, before cooling to room temperature over a period of 120 min. Upon removal from the reactor, each sample was rinsed with deionized water and blown dry using nitrogen gas.

To fabricate the devices, vacuum sputtering (EM SCD 500, Leica) was utilized to deposit several circle shaped Au spots with a diameter of 1.5 mm on the TNAs surface (Fig. 1), with an aluminum shadow mask. The duration of deposition was 360 s. Good adhesion of the Au electrodes was found.

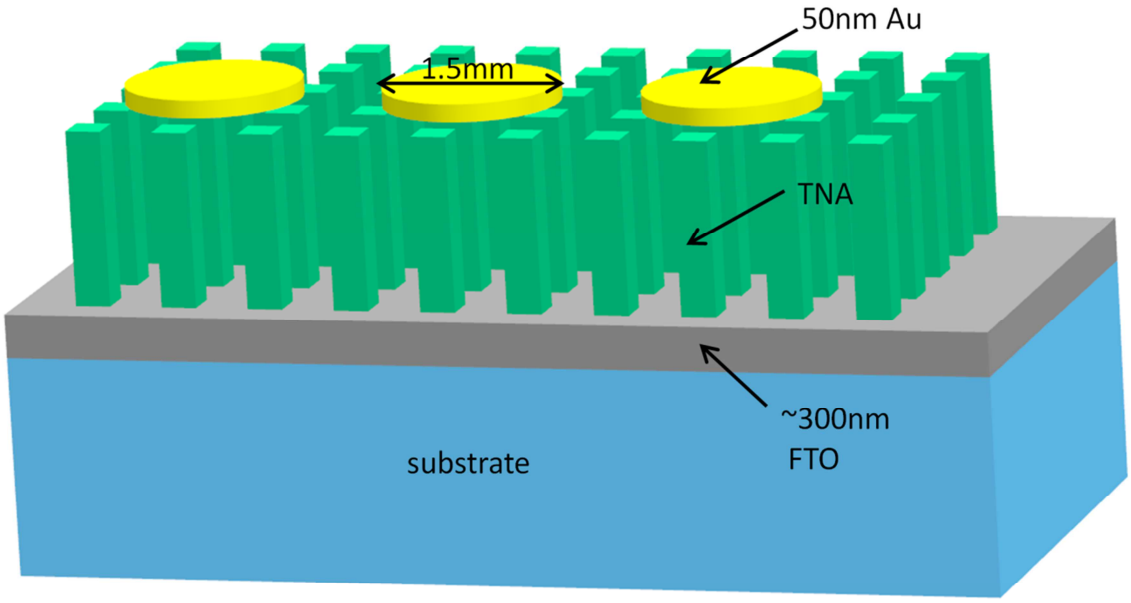

Fig. 1. Schematic diagram of memristor device based on Au/TNAs/FTO.

The morphology of the TNAs was examined by field emission scanning electron microscopy (SEM, Nova Nano SEM230). Transmission electron microscopy (TEM) and high resolution transmission electron microscopy (HRTEM) were carried out using an FEI TF20 electron microscope. X-ray diffraction analysis (XRD, Bruker Advance D8) was used to analyze the phase and crystal structure of the TNAs with Cu-Kα radiation (λ = 1.5418 Å). The surface chemical states of titanium and oxygen elements were characterized by X-ray photo-electron spectroscopy (XPS, Thermo Fisher Scientific, K-ALPHA). Electrical characterization of the devices was carried

out with an Agilent B1500A analyzer in sweep mode. The bias voltage was applied to the top Au electrode, and the FTO layer was connected with the ground electrode.

Results and discussion

Structural characterization

TEM images of an individual TiO_2 nanorod are shown in Fig. 2. A HRTEM image and selected area electron diffraction (SAED) pattern of the TiO_2 nanorod are shown as insets in Fig. 2. SEM images of TNAs prepared at the four temperatures used are shown in Fig. 3. The inset images show cross section views of the TNA layers from which the heights of the TNA layers were measured and are listed in Table 1. Each nanorod has a near square profile which grows larger with higher processing temperature and is accompanied a lengthening of the rod. It is evident that a single nanorod is made up of several nanowires of 10-15 nm diameter (Figs 3c and 3d). The shape of the rods is not dependent on the substrate, but on the bath solution [39, 40]. All the nanorods grow on a continuous layer of rutile which facilitates the initial nucleation and controls the density and vertical features. Furthermore, the intertwining of rods can increase the junction surface resulting in electron transfer channels [41, 42]. The average diameter of the nanorods was calculated for a 1 μm^2 area as highlighted in Fig. 3. The total number of nanorods in that square was used to

calculate the density of nanorods and the area ratio (*A*) of the TNAs was quantified using Eqn. 1. All values are summarized in Table 1.

$$A = \frac{\sum_{i=1}^{n} d_i^2}{l \times l} \quad (1)$$

where d is the diameter of a single nanorod, and *l* is the length of the highlighted area.

Table 1. Nanorod dimensions for TNAs prepared at four different temperatures (values are averages from 2 devices and 3 selected regions).

Temp. (K)	Number of nanorods per μm^2	Average diameter of single nanorod (nm)	Height of TNAs (μm)	Area ratio (%)
413	31	91	0.554	26
433	26	91	1.210	24
453	15	129	2.990	27
473	11	190	4.250	37

The height of the TNAs increases with increasing temperature, because the decomposition rate of titanium butoxide at higher temperatures is faster, and the nanowire combination and agglomeration is accelerated [43, 44].

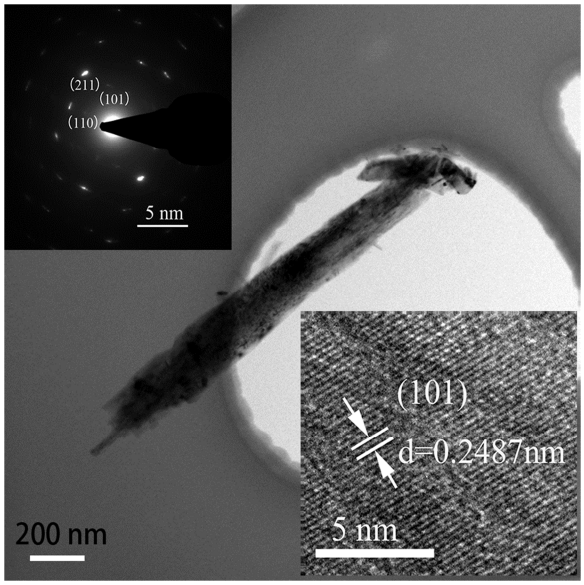

Fig. 2. TEM images of a single TiO_2 nanorod (upper inset: SAED pattern of the TiO_2 nanorod, lower inset: the HRTEM image of the TiO_2 nanorod).

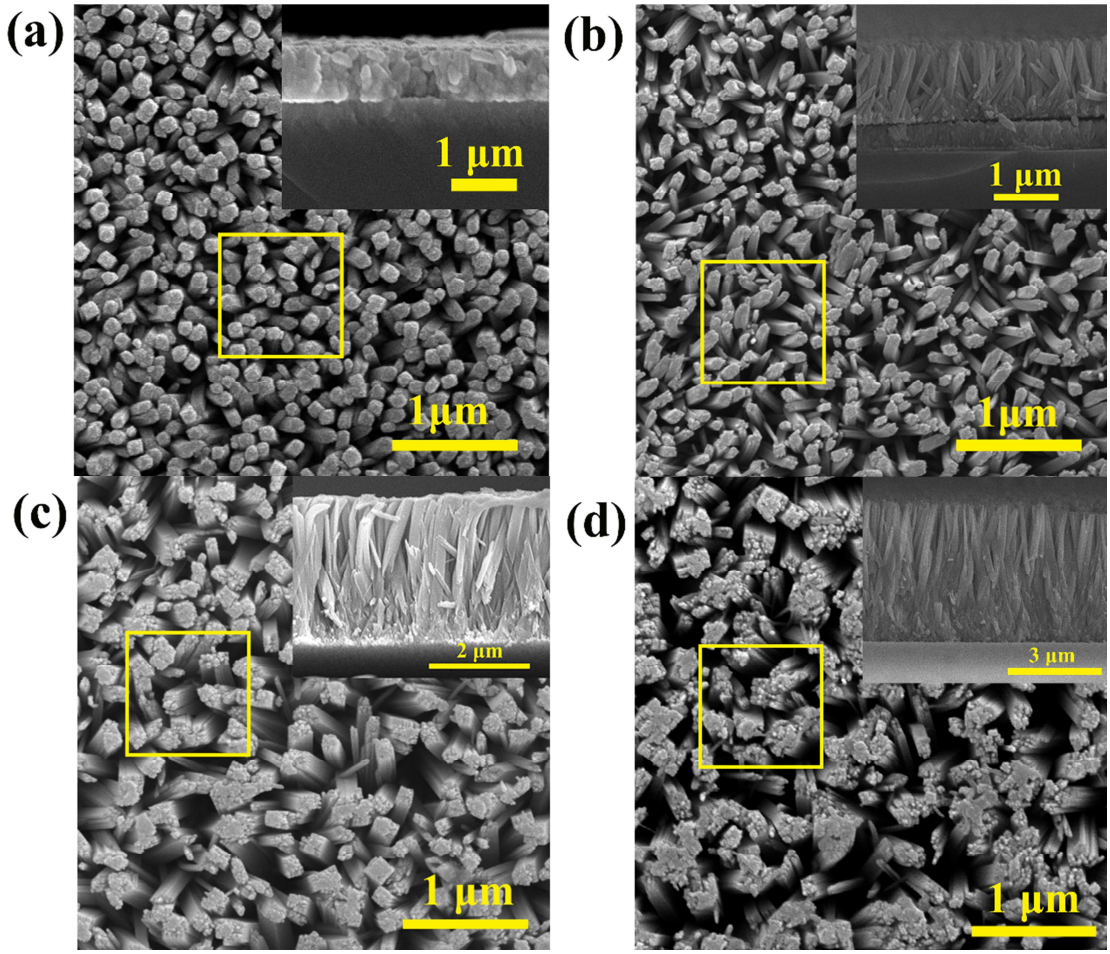

Fig. 3. SEM images of four TNAs morphologies, (a) 413K, (b) 433K, (c) 453K, and (d) 473K. Insets shown in all figures represent the cross section views of the TNAs layers.

Fig. 4 shows XRD patterns of the TNA samples prepared at different temperatures. All the patterns match the standard pattern for rutile (TiO_2, JCPDS, no. 21-1276). Weak peaks from the FTO substrate are also visible (SnO_2, JCPDS, no. 41-1445). With increasing temperature the peak intensities of the FTO substrate decrease, consistent with the increase in height of the TNAs with increasing temperature. Fig. 4 also shows that the TiO_2 (101) and (002) reflections are enhanced with increasing temperature. This is again consistent with increasing TNA height, with preferred orientation in the diffraction patterns indicating growth of the nanorods along the [001] direction perpendicular to the FTO substrate. These results agree with similar synthesis work in solar cell research [44].

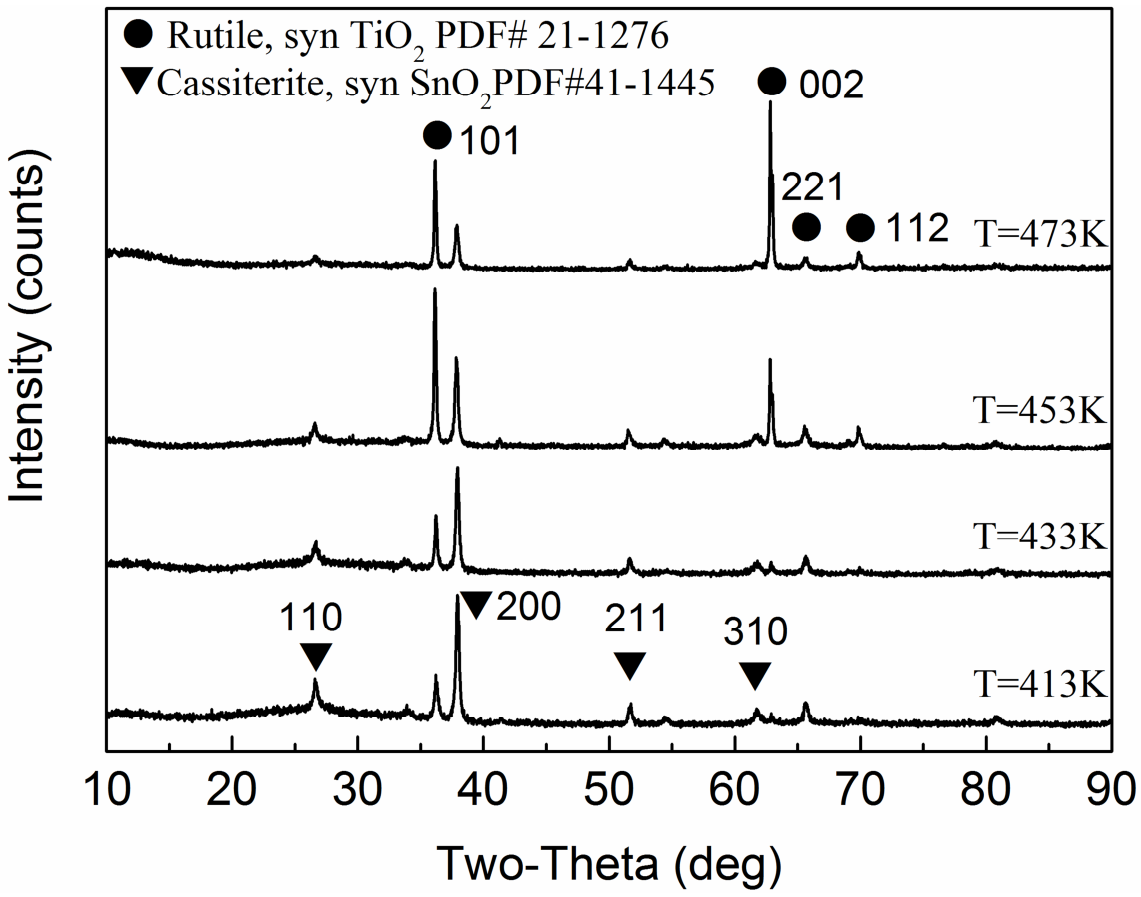

Fig. 4. XRD patterns of TNA layers synthesized at different temperatures on FTO glass substrates.

The chemical states of the TNA surfaces were investigated by XPS. The XPS survey spectra for TNA samples prepared at 413 K, 433 K, 453 K, and 473 K are shown in Fig. 5a. The patterns verify the presence of Ti, O and C (the latter from air contamination). High resolution XPS spectra covering the Ti 2p peaks are given in Fig. 5b. The Ti $2p_{1/2}$ (higher binding energy) and $2p_{3/2}$ (lower binding energy) peaks are evident with a separation of 5.7 eV. The Ti $2p_{3/2}$ binding energy of around 458.6 eV is in agreement with literature reported on TiO_2 [31], and is seen to increase with

increasing reaction temperature. This would be consistent with a small degree of Ti reduction to Ti^{3+} at higher reaction temperatures.

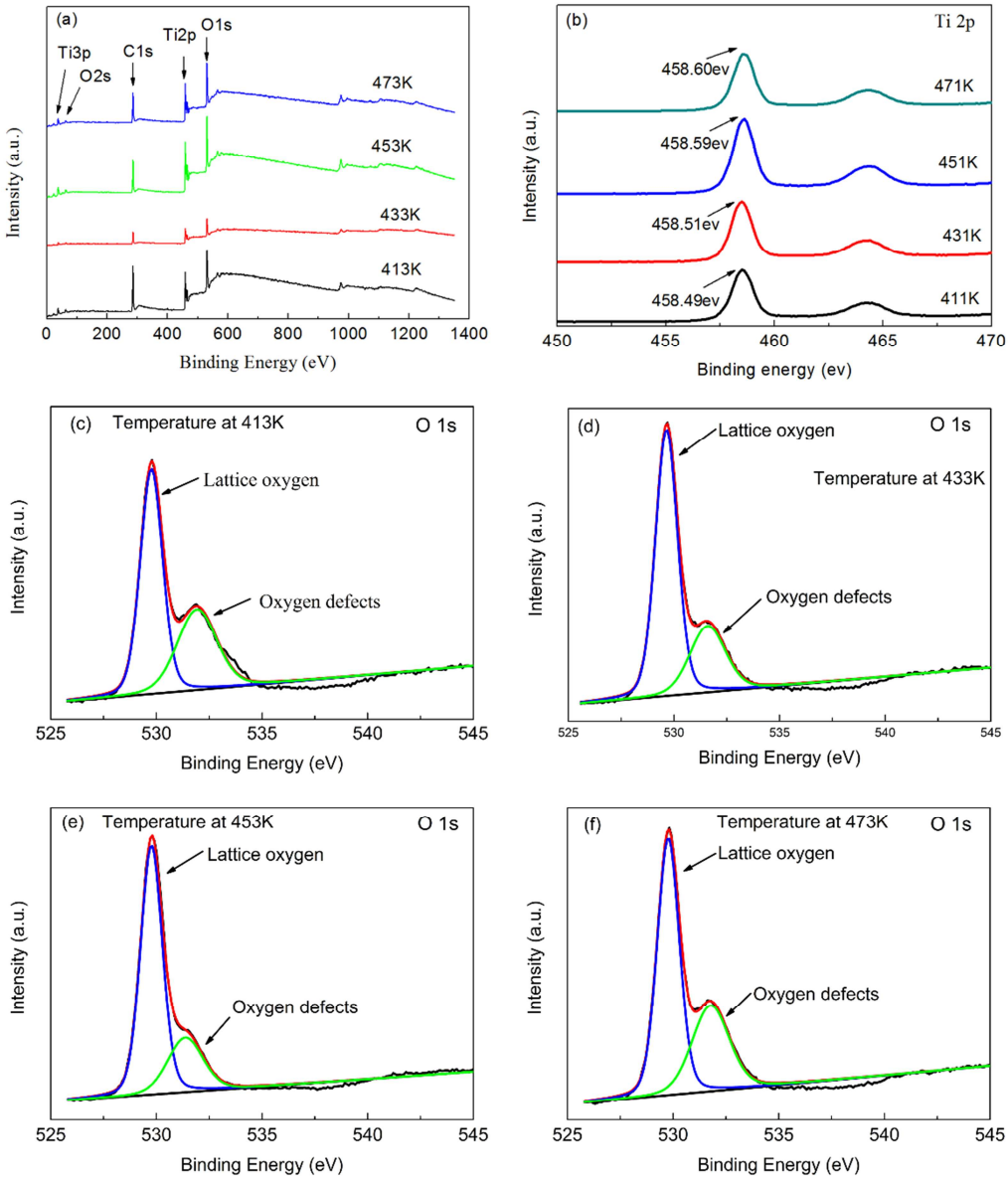

Fig. 5. XPS spectra of TNA layers synthesized at different temperatures showing (a) full survey spectra; (b) high resolution spectra for Ti 2p; high resolution spectra for O1s and the fitted spectra, (c) at 413 K, (d) at 433 K, (e) at 453 K and (f) at 473 K.

The high resolution O 1s spectra were fitted by two Gaussian peaks (see Figs. 5c-5f). The peak located at lower binding energy (529.7 eV) represents the lattice oxygen (i.e. oxygen bound to Ti^{4+}), while the other peak (531.2 eV) is attributed to oxygen defects on the nanorod surface [45], i.e. those oxygen atoms bound to Ti^{3+} [46], which is directly proportional to the number of oxygen vacancies. The peak position of the Ti-O bond shifts to higher energy as the synthesis temperature increases from 413 K to 473 K, which suggests the chemical state of Ti or O atoms change. The percentage of oxygen defects (listed in table 2), calculated according to the peak area and impact sensitivity factor [47], decreases with increasing synthesis temperature up to 453 K, followed by a significant increase at 473 K. This trend in oxygen defect concentration is related to the area ratio of the TNAs.

Table 2. The percentage of oxygen defects and lattice oxygen calculated from the XPS data.

Temperature (K)	Percentage (%)	
	Lattice oxygen (TiO_2)	Oxygen defects ($TiO_{1.5}$)
413	61.26	38.74
433	71.44	28.56
453	73.89	26.11
473	64.07	35.93

Electrical chracterization

For the electrical tests, the deposited gold served as the top electrode and the FTO as the grounded bottom electrode. Current-voltage (I-V) hysteresis loops of devices based on the TNA layers prepared at different temperatures are shown in Fig. 6, with the semi-logarithmic I-V characteristics inset (further cycles are given in the supporting information as Fig. S1). The devices are denoted S1, S2, S3 and S4 for those TNAs prepared at 413, 433, 453 and 473 K, respectively. All four devices display bipolar resistive characteristics over the range -4 V to 2 V. Device S4 shows an I-V loop more typical of TiO_x devices, while those for devices S1, S2 and S3 are quite different [11, 37]. For device S1 (Fig. 6a), as the voltage firstly sweeps form 0 to -4 V, three ranges in the current curve can be defined. In the first range, from 0 to -1.29 V, the response current maintains a near constant value. From -1.29 V to -2.27 V, an exponential increase in current is observed. In the final step (-2.27 V to -3.46 V), the current increase is sharper until reaching the compliance current of 1 mA at -3.46 V. On reversing the voltage from -4 V to 0, the current continuously decreased from 10^{-4} A to 10^{-6} A. The results are similar for the other three devices, though the strength of current and the area of the hysteresis loop are different.

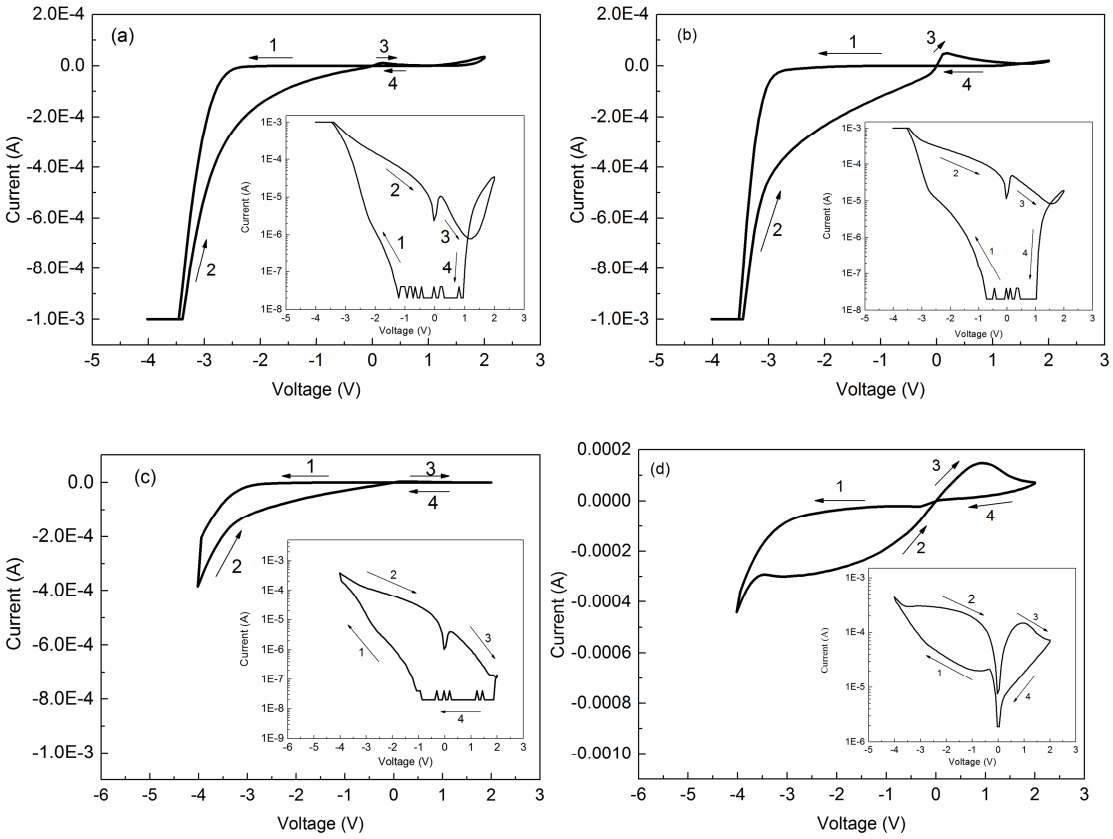

Fig. 6. Typical hysteresis I-V curves of Au/TNAs/FTO devices containing TNAs synthesized at: (a) 413 K (S1), (b) 433 K (S2), (c) 453 K (S3) and (d) 473 K (S4). Semi-log I-V curves are inset.

The current at -3 V during the setting process (0 to -4 V) and the voltage at which the devices transform from the high resistance state (HRS) to the low resistance state (LRS, resistance < 100 kΩ) are listed in Table 3. The current values at -3 V on setting are found to decrease with increasing temperature of TNA synthesis, while the voltage values at which the devices reach the LRS increase with increasing temperature of TNA synthesis. In the case of the device S4, the current at -3 V was higher than that for devices S2 and S3 and it was at the LRS throughout the measurement. As seen in Table 1, the TNA area ratios decrease with increasing

reaction temperature from 413 K to 453 K and would be consistent with the decreasing current at -3 V.

The observed electrical behavior can be explained by considering the changes in oxygen vacancy concentration. With increasing temperature of the hydrothermal process, the concentration of oxygen defects decreases up to 453 K, and is correlated with the observed decrease in current for the set process of devices S1, S2 and S3. Oxygen vacancies play an important role in the conduction of materials [12], acting as electron traps and allowing for the formation of conducting channels. The current at -3 V for the device S4 is seen to increase with respect to that for device S3, consistent with the observed increase in oxygen defect concentration between TNAs prepared at 473 K and 453 K (Table 2). However, despite the similarities in defect concentration between the samples prepared at 413 and 473 K, the devices based on these TNAs show very different currents at -3 V. This suggests that not only is defect concentration an important factor, but that the resistance associated with TNA height is also a significant factor. Indeed previous studies on thin films have shown that film thickness is inversely related to current [23]. In the present work this relationship is also found in devices S1 to S3. However, in the case of device S4, which has the tallest nanorods, the current increases slightly due to the increase in oxygen vacancy concentration. Additionally, device S4 exhibits poor switching behavior with only a small difference between LRS and HRS. The results suggest that oxygen vacancy

concentration is the primary factor responsible for the set current and that a TNA height of around. 3 μm or less is required for significant bipolar switching.

Table 3. The current at -3 V during the setting process (0 to -4 V) and the voltage at which devices S1 to S4 transform from high resistance state (HRS) to the low resistance state (LRS, resistance < 100 kΩ). Values are averages from 2 devices.

Samples	The current value when the voltage is -3 V (A)	The voltage value when the resistance is reduced to 100 kΩ (V)
S1	22.06×10^{-5}	-2.62
S2	5.61×10^{-5}	-2.90
S3	1.31×10^{-5}	-3.25
S4	8.30×10^{-5}	-

Based on the resistive switching behavior, several popular mechanisms can be used to fit the domain current, corresponding to applied voltage or electric field. These mechanisms include, (i) Poole-Frenkel emission [48]; (ii) Schottky emission [49]; (iii) space charge limited current (SCLC) [50, 51] and (iv) Fowler-Nordheim Tunneling [52]. Since the memristors in the current work are based on TNAs with abundant oxygen defects, the SCLC mechanism can be used to explain the I-V loops. This mechanism has been used to account for the conduction mechanism in other TNA

based sandwich structures [31]. In the SCLC mechanism, oxygen vacancies act as electron traps, which can diffuse through the material and trigger the formation of further oxygen vacancies under an external applied voltage [53].

The retention time in HRS and LRS of the 4 devices was measured and is shown in the supporting information in Fig. S2. In HRS the retention times for all devices are above 2000 ms. For the devices S1, S2 and S3, the LRS retention time decreases with decreasing oxygen vacancy concentration and increasing nanorod height. It is reported that long retention times are associated with potential wells or deep traps which prevent the trapped electrons escaping [54]. Device S4 exhibits the longest LRS retention time. The TNAs in the device exhibited defect concentrations similar to those in device S1, but with a much larger area ratio. The results show that the relationship between retention time, area ratio and oxygen vacancy concentration is complicated.

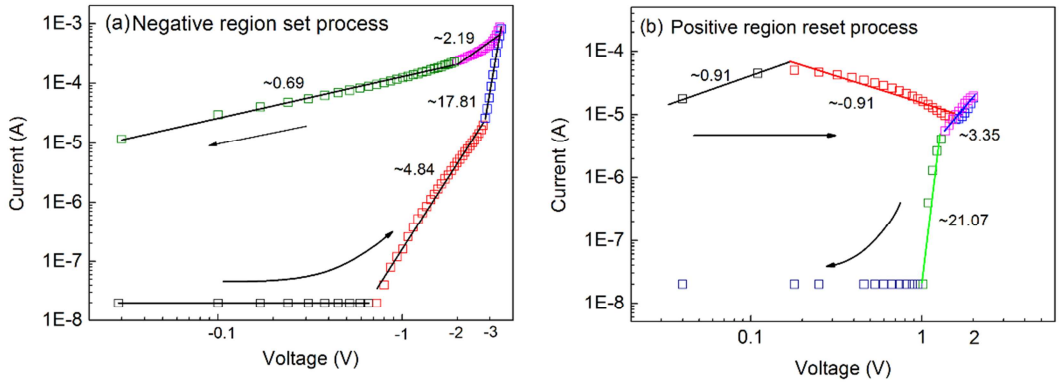

Fig. 7. Fits to log (I)-log (V) curves of the S2 device based on TNAs synthesized at 433 K, using the SCLC model, showing (a) the set process and (b) the reset process. Fitted slopes are indicated.

The fitted log (I) vs log (V) curves for the S2 using the SCLC model are shown in Fig. 7. When the voltage sweeps from 0 to -4 V, the curve shows three steps as described above and can be fitted to lines of different slope. While the negative voltage carried on the top electrode is small (less than 0.73 V in this case), the Schottky barrier at the Au/TNA interface constrains the electron transport, which is caused by the difference between the work function of the Au top electrode (5.1 eV) and the Fermi level of rutile TiO_2 (4.2 eV). The Fermi level of the interface is closer to that of rutile. The barrier limits the diffusion of electrons and oxygen vacancies. So the device shows a small rectifying current and stays in the HRS. The initial process is associated with the Ohmic contact and the current is attributed to the thermally generated free carriers [55]. Lattice vibrations caused by Joule heating and long electron diffusion distances could explain the low current observed in the studied device. When the sweep voltage is higher than the threshold voltage in the trap filled limiting region, the current significantly increased in response with a slope much greater than 2.0 (the theoretical value from Mott's Law) in the log (I)-log (V) plot. This type of deviation from Mott's law in the transition region has been previously been attributed to the dynamic evolution of oxygen vacancies under bias polarization [56, 57]. The filled traps create channels for

rapid electron transport. After the first channel is generated, further traps are filled and the device switches from HRS to LRS. At the end of the set process, there is an acceleration of trap filling, which is attributed to the triggering of new vacancies. Under a high enough bias, new vacancies are triggered and act as additional traps to enlarge the conducting channels and increase the current [58]. When the voltage was swept from -4 V to -1.92 V, the slope of ~2.19 in the log (I) vs log (V) plot suggests that the traps remain virtually fully filled. As the voltage was swept from -1.92 V to 0 V, the slope was 0.69 and a resistance of around $10^4\ \Omega$ was maintained (LRS). In the reset process, initially a slope of nearly 1 is observed up to 0.18 V, confirming traps are filled. Above 0.18 V the slope is reversed as electrons flow from the traps and the device gradually switches from LRS to HRS. At higher voltages up to 2 V a large slope of 3.35 is seen, indicating that the negative bias carried on the Au top electrode forces the electrons to leave the traps more rapidly as more traps empty. As the voltage is reduced, the device in its HRS state forces a sharp reduction in current, until reaching an almost constant current at around 1 V. On reversing the bias, electrons are transported from the bottom FTO electrode to top the Au electrode, and the filled traps lose their electrons and become barriers again. Eventually, the device returns to its initial HRS state.

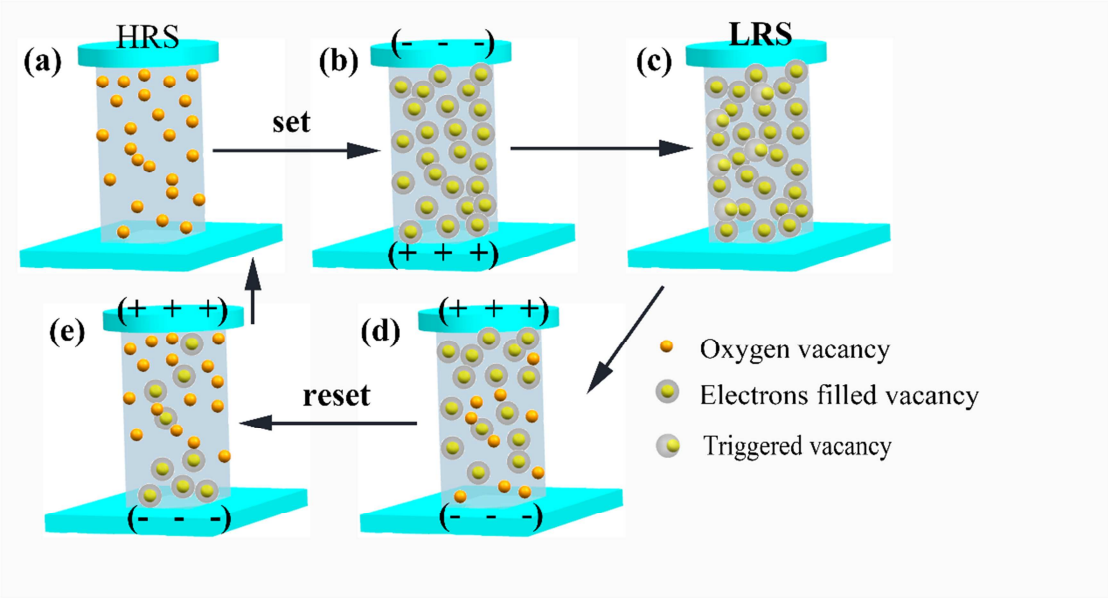

Fig. 8. Schematic diagram showing changes in electron trapping by oxygen vacancies during set and rest processes in Au/TNA/FTO memristor devices.

A schematic model for the electron trapping behavior in the studied devices based on the SCLC mechanism in shown in Fig. 8. As can be seen in Fig. 8a, the initial state of the device is in HRS and the oxygen vacancies of the as prepared TNAs are distributed randomly. When a small bias (either negative or positive) is applied on the top Au electrode, the device possesses a very small rectifying current in the order of 10 nA. Although the tiny bias is not enough to switch the resistance state of the device, there is a small potential gradient and gradually this overcomes the interface Schottky barrier and forces the electrons to fill the oxygen vacancies. Here the oxygen vacancies act as traps and can be regarded as electron reservoirs which can transform from the empty state (lack of electrons) to the full state (filled electrons) [23]. It is noted here that the oxygen vacancies themselves are unlikely to show significant

diffusion. As the oxygen vacancies become filled with electrons they form channels through which current can flow, increasing rapidly, with more vacancies around the channel becoming filled (Fig. 8b). In addition, the filled traps can trigger formation of new vacancies, enhancing the conduction channel. This results in a sharp increase in current in the later period of the setting process. This phenomenon can be readily understood using a simple analogy of a stream flowing through a channel, as the flow of water increases, the banks of the channel are eroded and collapse, widening the channel and increasing the flow. After most of the intrinsic vacancies are filled by electrons, the device switches to the LRS and with Ohmic contact behavior (Fig. 8c). On reversing the bias, filled vacancies away from the channels can release electrons preferentially. However, the diffusion distance is such that they make little impact on the current, with values in the order of 10^4 Ω. In the case of a positive bias, triggered and intrinsic vacancies empty successively (Fig. 8d). The conductive channels of traps become disrupted and the de-trapping process is accelerated (Fig. 8e). When most of the vacancies recover to their empty state, the device returns to HRS and exhibits a small rectifying behavior (Fig. 8a).

Conclusions

Bipolar memristor devices of the type Au/TNA/FTO with different TNA morphologies were prepared and investigated. The height and area ratio of the TNAs were found to affect oxygen vacancy concentration and in turn memristive behavior.

The area ratio of the TNAs decreased with increasing synthesis temperature from 413 K to 433 K, but then increased at 473 K, while the oxygen defect concentration decreased with increasing TNA height up to around 3 μm. Devices based on TNAs of this height or less showed good memristive performance, while those containing TNAs of 4.25 μm showed little difference between the low resistive and high resistive states. The current-voltage behavior of these TNA based devices was investigated in detail and explained by the SCLC mechanism. A small rectifying current is observed under small bias. A large increase in current at the end of the setting process is attributed to the creation of new vacancies (triggered vacancies).

Conflicts of interest

There are no conflicts of interest to declare.

Acknowledgments

The work was supported by the National Defense Science and Technology Innovation Project Grant No. 1716313ZT01002601 and Grant No. 1716313ZT009052001; and the Science and Technology Plan Project of Hunan Province Grant No. 2015TP1007; Initial Research Funding for Special Associate Professor by Central South University Grant No. 202045002; National Natural Science Foundation for Young Scientists of China No. 51802353; National Natural Science Foundation for Young Scientists of China No. 51602350.

References

[1] L.-Y. Chen, Z. Yang, C.-Y. Chen, T.-Y. Ho, P.-W. Liu, H.-T. Chang, Cascade quantum dots sensitized TiO_2 nanorod arrays for solar cell applications, Nanoscale, 3 (2011) 4940.

[2] D.S. Conceição, C.A.L. Graça, D.P. Ferreira, A.M. Ferraria, I.M. Fonseca, A.M. Botelho do Rego, A.C.S.C. Teixeira, L.F. Vieira Ferreira, Photochemical insights of TiO2 decorated mesoporous SBA-15 materials and their influence on the photodegradation of organic contaminants, Microporous and Mesoporous Materials, 253 (2017) 203-214.

[3] F. Hong, J. Zhou, C. Liu, F. Yang, C. Wu, L. Zheng, P. Yang, Effect of Nano-TiO_2 on Photochemical Reaction of Chloroplasts of Spinach, Biological Trace Element Research, 105 (2005) 269-279.

[4] S. Hoang, S. Guo, N.T. Hahn, A.J. Bard, C.B. Mullins, Visible light driven photoelectrochemical water oxidation on nitrogen-modified TiO_2 nanowires, Nano Lett., 12 (2012) 26-32.

[5] R. Guo, H. Luo, W. Liu, X. Zhou, L. Tang, K. Zhou, D. Zhang, High energy density in PVDF nanocomposites using an optimized nanowire array, Phys. Chem. Chem. Phys., 20 (2018) 18031-18037.

[6] S. Sun, H. Ding, X. Hou, D. Chen, S. Yu, H. Zhou, Y. Chen, Effects of organic modifiers on the properties of TiO_2-coated $CaCO_3$ composite pigments prepared by the hydrophobic aggregation of particles, Appl. Surf. Sci., 456 (2018) 923-931.

[7] B. Liu, E.S. Aydil, Growth of Oriented Single-Crystalline Rutile TiO_2 Nanorods on Transparent Conducting Substrates for Dye-Sensitized Solar Cells, J. Am. Chem. Soc. , 131 (2009) 3985-3990.

[8] J. Liang, G. Zhang, J. Yang, W. Sun, M. Shi, TiO2 hierarchical nanostructures: Hydrothermal fabrication and application in dye-sensitized solar cells, AIP Advances, 5 (2015) 017141.

[9] G.K. Mor, K. Shankar, M. Paulose, O.K. Varghese, C.A. Grimes, Use of Highly-Ordered TiO_2 Nanotube Arrays in Dye-Sensitized Solar Cells, Nano Lett., 6 (2006) 215-218.

[10] E.M. Vogel, Technology and metrology of new electronic materials and devices, Nature Nanotechnology, 2 (2007) 25-32.

[11] L. Chua, If it’s pinched it’s a memristor, Semicond. Sci. Technol., 29 (2014) 104001-104043.

[12] K. Szot, M. Rogala, W. Speier, Z. Klusek, A. Besmehn, R. Waser, TiO2-a prototypical memristive material, Nanotechnology, 22 (2011) 254001.

[13] W.Y. Park, G.H. Kim, J.Y. Seok, K.M. Kim, S.J. Song, M.H. Lee, C.S. Hwang, A Pt/TiO_2/Ti Schottky-type selection diode for alleviating the sneak current in resistance switching memory arrays, Nanotechnology, 21 (2010) 195201.

[14] F. Zhang, X. Gan, X. Li, L. Wu, X. Gao, R. Zheng, Y. He, X. Liu, R. Yang, Realization of rectifying and resistive switching behaviors of TiO_2 nanorod arrays for nonvolatile memory, Electrochem. Solid-State Lett., 14 (2011) H422-H425.

[15] X. Zhang, S. Liu, X. Zhao, F. Wu, Q. Wu, W. Wang, R. Cao, Y. Fang, H. Lv, S. Long, Q. Liu, M. Liu, Emulating short-term and long-term plasticity of bio-synapse based on Cu/a-Si/Pt memristor, IEEE Electron. Device Lett., 38 (2017) 1208-1211.

[16] J.Y. Chen, C.L. Hsin, C.W. Huang, C.H. Chiu, Y.T. Huang, S.J. Lin, W.W. Wu, L.J. Chen, Dynamic evolution of conducting nanofilament in resistive switching memories, Nano Lett., 13 (2013) 3671-3677.

[17] K.J. Yoon, M.H. Lee, G.H. Kim, S.J. Song, J.Y. Seok, S. Han, J.H. Yoon, K.M. Kim, C.S. Hwang, Memristive tri-stable resistive switching at ruptured conducting filaments of a Pt/TiO_2/Pt cell, Nanotechnology, 23 (2012) 185202-185209.

[18] S. Boyn, J. Grollier, G. Lecerf, B. Xu, N. Locatelli, S. Fusil, S. Girod, C. Carretero, K. Garcia, S. Xavier, J. Tomas, L. Bellaiche, M. Bibes, A. Barthelemy, S. Saighi, V. Garcia, Learning through ferroelectric domain dynamics in solid-state synapses, Nat. Commun., 8 (2017) 14736.

[19] D. Ielmini, F. Nardi, C. Cagli, Physical models of size-dependent nanofilament formation and rupture in NiO resistive switching memories, Nanotechnology, 22 (2011) 254022.

[20] Z. Fan, X. Fan, A. Li, L. Dong, In situ forming, characterization, and transduction of nanowire memristors, Nanoscale, 5 (2013) 12310-12315.

[21] D.B. Strukov, G.S. Snider, D.R. Stewart, R.S. Williams, The missing memristor found, Nature, 453 (2008) 80-83.

[22] Q. Xia, J.J. Yang, W. Wu, X. Li, R.S. Williams, Self-aligned memristor cross-point arrays fabricated with one nanoimprint lithography step, Nano Lett., 10 (2010) 2909-2914.

[23] T.D. Dongale, S.S. Shinde, R.K. Kamat, K.Y. Rajpure, Nanostructured TiO_2 thin film memristor using hydrothermal process, J. Alloys Compd., 593 (2014) 267-270.

[24] K. Nagashima, T. Yanagida, M. Kanai, K. Oka, A. Klamchuen, S. Rahong, G. Meng, M. Horprathum, B. Xu, F. Zhuge, Y. He, T. Kawai, Switching properties of titanium dioxide nanowire memristor, Japanese, J. Appl. Phys., 51 (2012) 11PE09.

[25] B. Sun, Q.L. Li, W.X. Zhao, H.W. Li, L.J. Wei, P. Chen, White-light-controlled resistance switching in TiO_2/α-Fe_2O_3 composite nanorods array, J. Nanopart. Res., 16 (2014) 2389-2394.

[26] C.J. O'Kelly, J.A. Fairfield, D. McCloskey, H.G. Manning, J.F. Donegan, J.J. Boland, Associative enhancement of time correlated response to heterogeneous stimuli in a neuromorphic nanowire device, Adv. Electron. Mater., 2 (2016) 1500458.

[27] R. Waser, M. Aono, Nanoionics-based resistive switching memories, Nature Mater., 6 (2007) 833-840.

[28] R. Schmitt, J. Spring, R. Korobko, J.L.M. Rupp, Design of Oxygen Vacancy Configuration for Memristive Systems, ACS Nano, 11 (2017) 8881-8891.

[29] S.-G. Park, B. Magyari-Kope, Y. Nishi, Impact of oxygen vacancy ordering on the formation of a conductive filament in TiO_2 for resistive switching memory, IEEE Electron. Device Lett., 32 (2011) 197-199.

[30] Y. H. Do, J. S. Kwak, Y. C. Bae, K. H. Jung, H. S. Im, J. P. Hong, Hysteretic bipolar resistive switching characteristics in TiO_2/TiO_{2-x} multilayer homojunctions, Appl. Phys. Lett., 95 (2009) 093507

[31] M. Xiao, K.P. Musselman, W.W. Duley, Y.N. Zhou, Reliable and low-power multilevel resistive switching in TiO_2 nanorod arrays structured with a TiO_x seed layer, ACS Appl. Mater. Interfaces, 9 (2017) 4808-4817.

[32] J.-H. Lee, I.-C. Leu, M.-C. Hsu, Y.-W. Chung, M.-H. Hon, Fabrication of aligned TiO_2 one-dimensional nanostructured arrays using a one-step templating solution approach, J. Phys. Chem. B, 109 (2005) 13056-13059.

[33] A. Kumar, A.R. Madaria, C. Zhou, Growth of aligned single-crystalline rutile TiO_2 nanowires on arbitrary substrates and their application in dye-sensitized solar cells, J. Phys. Chem. C 114 (2010) 7787-7792.

[34] A. Ramadoss, S.J. Kim, Vertically aligned TiO_2 nanorod arrays for electrochemical supercapacitor, J. Alloys Compd., 561 (2013) 262-267.

[35] M. Iraj, F.D. Nayeri, E. Asl-Soleimani, K. Narimani, Controlled growth of vertically aligned TiO_2 nanorod arrays using the improved hydrothermal method and their application to dye-sensitized solar cells, J. Alloys Compd., 659 (2016) 44-50.

[36] J.-N. Nian, H. Teng, Hydrothermal synthesis of single-crystalline anatase TiO_2 nanorods with nanotubes as the precursor, J. Phys. Chem. B, 110 (2006) 4193-4198.

[37] K.M. Kim, B.J. Choi, M.H. Lee, G.H. Kim, S.J. Song, J.Y. Seok, J.H. Yoon, S. Han, C.S. Hwang, A detailed understanding of the electronic bipolar resistance switching behavior in Pt/TiO_2/Pt structure, Nanotechnology, 22 (2011) 254010.

[38] J.J. Yang, M.D. Pickett, X. Li, D.A. Ohlberg, D.R. Stewart, R.S. Williams, Memristive switching mechanism for metal/oxide/metal nanodevices, Nature Nanotechnol. 3 (2008) 429-433.

[39] X. Feng, K. Shankar, O.K. Varghese, M. Paulose, T.J. Latempa, C.A. Grimes, Vertically aligned single crystal TiO_2 nanowire arrays grown directly on transparent conducting oxide coated glass: synthesis details and applications, Nano Lett., 8 (2008) 3781-3786.

[40] X. Feng, K. Zhu, A.J. Frank, C.A. Grimes, T.E. Mallouk, Rapid charge transport in dye-sensitized solar cells made from vertically aligned single-crystal rutile TiO_2 nanowires, Angew. Chem., 124 (2012) 2781-2784.

[41] Z. Wei, Y. Yao, T. Huang, A. Yu, Solvothermal growth of well-aligned TiO_2 nanowire arrays for dye-sensitized solar cell: dependence of morphology and vertical orientation upon substrate pretreatment, Int. J. Electrochem. Sci., 6 (2011) 1871 - 1879.

[42] Y. Zhang, C. Han, G. Zhang, D.D. Dionysiou, M.N. Nadagouda, PEG-assisted synthesis of crystal TiO_2 nanowires with high specific surface area for enhanced photocatalytic degradation of atrazine, Chem. Eng. J., 268 (2015) 170-179.

[43] E. Hosono, S. Fujihara, K. Kakiuchi, H. Imai, Growth of submicrometer-scale rectangular parallelepiped rutile TiO_2 films in aqueous $TiCl_3$ solutions under hydrothermal conditions, J. Am. Chem. Soc., 106 (2004) 7790-7791.

[44] J. Yu, G. Wang, B. Cheng, M. Zhou, Effects of hydrothermal temperature and time on the photocatalytic activity and microstructures of bimodal mesoporous TiO_2 powders, Appl. Catal. , B, 69 (2007) 171-180.

[45] M. Ghaffari, M.B. Cosar, H.I. Yavuz, M. Ozenbas, A.K. Okyay, Effect of Au nano-particles on TiO_2 nanorod electrode in dye-sensitized solar cells, Electrochimica Acta, 76 (2012) 446-452.

[46] B. Bharti, S. Kumar, H.N. Lee, R. Kumar, Formation of oxygen vacancies and Ti^{3+} state in TiO_2 thin film and enhanced optical properties by air plasma treatment, Sci. Rep., 6 (2016) 32355.

[47] Y. Zhu, M. Li, H. Zhou, Z. Hu, X. Liu, X. Fang, B. Sebo, G. Fang, X. Zhao, Nonvolatile bipolar resistive switching in an $Ag/TiO_2/Nb:SrTiO_3/In$ device, J. Phys. D: Appl. Phys., 45 (2012) 375303.

[48] H. Hirashima, Y. Watanabe, T. Yoshida, Switching of TiO2-V2O5-P2O5 glasses, J. Non-Cryst. Solids, 95 (1987) 825-832.

[49] T. You, N. Du, S. Slesazeck, T. Mikolajick, G. Li, D. Buerger, I. Skorupa, H. Stoecker, B. Abendroth, A. Beyer, K. Volz, O.G. Schmidt, H. Schmidt, Bipolar Electric-Field Enhanced Trapping and Detrapping of Mobile Donors in BiFeO3 Memristors, ACS Appl. Mater. Interfaces, 6 (2014) 19758-19765.

[50] Y.D. Xia, W.Y. He, L. Chen, X.K. Meng, Z.G. Liu, Field-induced resistive switching based on space-charge-limited current, Appl. Phys. Lett., 90 (2007) 022907-022909.

[51] T. Harada, I. Ohkubo, K. Tsubouchi, H. Kumigashira, T. Ohnishi, M. Lippmaa, Y. Matsumoto, H. Koinuma, M. Oshima, Trap-controlled space-charge-limited current mechanism in resistance switching at $Al/Pr_{0.7}Ca_{0.3}MnO_3$ interface, Appl. Phys. Lett., 92 (2008) 222113.

[52] E.W. Lim, R. Ismail, Conduction Mechanism of Valence Change Resistive Switching Memory: A Survey, Electronics, 4 (2015) 586-613.

[53] X.W. He, Y.L. Yin, J. Guo, H.J. Yuan, Y.H. Peng, Y. Zhou, D. Zhao, K. Hai, W.C. Zhou, D.S. Tang, Memristive properties of hexagonal WO_3 nanowires induced by oxygen vacancy migration, Nanoscale Res. Lett., 8 (2013).

[54] H. Schroeder, V.V. Zhirnov, R.K. Cavin, R. Waser, Voltage-time dilemma of pure electronic mechanisms in resistive switching memory cells, J. Appl. Phys., 107 (2010) 054517.

[55] W. Xu, Y. Lee, S.Y. Min, C. Park, T.W. Lee, Simple, inexpensive, and rapid approach to fabricate cross-Shaped memristors using an inorganic-nanowire-digital-alignment technique and a one-step reduction process, Adv. Mater., 28 (2016) 527-532.

[56] W.F. Pasveer, J. Cottaar, C. Tanase, R. Coehoorn, P.A. Bobbert, P.W.M. Blom, D.M. de Leeuw, M.A.J. Michels, Unified description of charge-carrier mobilities in disordered semiconducting polymers, Phys. Rev. Lett., 94 (2005) 206601.

[57] X.G. Zhang, S.T. Pantelides, Theory of space charge limited currents, Phys. Rev. Lett., 108 (2012) 266602.

[58] J. Joshua Yang, F. Miao, M.D. Pickett, D.A. Ohlberg, D.R. Stewart, C.N. Lau, R.S. Williams, The mechanism of electroforming of metal oxide memristive switches, Nanotechnology, 20 (2009) 215201.